PNAS RESEARCH ARTICLE | MICROBIOLOGY OPEN ACCESS

# Pleural macrophages translocate to the lung during infection to promote improved influenza outcomes

James P. Stumpff II[a], Sang Yong Kim[b], Matthew I. McFadden[c,d], Andrew Nishida[e], Roksana Shirazi[a], Yael Steuerman[f], Irit Gat-Viks[f], Adriana Forero[c,d], Meera G. Nair[b], and Juliet Morrison[a,1]

Edited by Peter Palese, Icahn School of Medicine at Mount Sinai, New York, NY; received January 10, 2023; accepted October 30, 2023

**Seasonal influenza results in 3 to 5 million cases of severe disease and 250,000 to 500,000 deaths annually. Macrophages have been implicated in both the resolution and progression of the disease, but the drivers of these outcomes are poorly understood. We probed mouse lung transcriptomic datasets using the Digital Cell Quantifier algorithm to predict immune cell subsets that correlated with mild or severe influenza A virus (IAV) infection outcomes. We identified a unique lung macrophage population that transcriptionally resembled small serosal cavity macrophages and whose presence correlated with mild disease. Until now, the study of serosal macrophage translocation in the context of viral infections has been neglected. Here, we show that pleural macrophages (PMs) migrate from the pleural cavity to the lung after infection with IAV. We found that the depletion of PMs increased morbidity and pulmonary inflammation. There were increased proinflammatory cytokines in the pleural cavity and an influx of neutrophils within the lung. Our results show that PMs are recruited to the lung during IAV infection and contribute to recovery from influenza. This study expands our knowledge of PM plasticity and identifies a source of lung macrophages independent of monocyte recruitment and local proliferation.**

influenza | pleural cavity | macrophages | transcriptomics | tissue deconvolution

## Significance

The immune responses that drive influenza outcomes are not fully characterized. Furthermore, the pleural cavity, which surrounds the lungs and contains immune cells, has not been well studied in the context of influenza. We used lung gene expression data from mouse models of mild and severe influenza to predict immune cell differences that associate with different disease outcomes. Pleural macrophages were predicted to be a positive correlate of mild disease. We established a mouse model of influenza disease and used it to show that pleural macrophages migrate to the lungs of infected mice to decrease disease severity. This study expands our knowledge of PM plasticity and provides a new source of lung macrophages that impact influenza outcomes.

Influenza A virus (IAV) is responsible for seasonal epidemics and several pandemics that arose from a lack of immunity and human-to-human transmission (1). Despite current vaccine strategies, IAV remains a major public health concern. Patient outcomes of IAV infections depend on the delicate balance between immune protection and immunopathology that is orchestrated by innate immune responses and subsequent adaptive immunity (2). Further investigation into influenza outcomes is needed to understand the resolution of viral clearance and restoration of pulmonary homeostasis.

The host response to infection is an important determinant of influenza outcomes (3–7). For example, severe influenza outcomes are associated with high levels of proinflammatory cytokines and leukocytes in the lung (5, 7, 8). Patients hospitalized with severe seasonal influenza infections have a sustained increase in monocytes (9), and patients with severe avian influenza have elevated levels of inflammatory cytokines in their acute-phase sera (10–12). Infection with highly pathogenic IAVs such as the 1918 virus and avian H5N1 virus leads to a massive recruitment of neutrophils and inflammatory macrophages to the lungs of mice (3, 4). Depending on the virus strain, mice may develop progressive pneumonia characterized by extensive neutrophilia, hypercytokinemia, pulmonary edema, and reductions in alveolar gas exchange that are reminiscent of acute respiratory distress (ARDS) in human patients (13–16). We previously identified lung transcriptomic signatures that distinguished mild and severe influenza outcomes in BALB/c mice infected with different IAV strains (17). A three-pronged lung signature consisting of decreased expression of lipid metabolism and coagulation genes and increased expression of proinflammatory cytokine genes was identified in mice that had succumbed to infection, while a signature of increased expression of lipid metabolism and coagulation genes and lower expression of proinflammatory cytokine genes was identified in mice that recovered from infection (17).

Serous membranes support and protect the internal organs of all vertebrate animals. Each serous membrane consists of two layers separated by a thin, fluid-filled serosal cavity. The serosal cavity that envelops the lungs is called the pleural cavity, while the cavities that surround the abdominal organs and the heart are known as the peritoneal cavity and the pericardial cavity, respectively. Serosal cavities contain multiple immune cells including innate B cells and T cells, but macrophages are a prominent cell population. Serosal macrophages are divided into small and large macrophages based on their cell size and surface marker expression. Small serosal macrophages are $MHCII^{+}F4/80^{-}$ and constitute ~10% of serosal macrophages, while large serosal macrophages are $MHCII^{-}F4/80^{+}$ and

Author contributions: J.M. designed research; J.P.S., S.Y.K., A.N., R.S., Y.S., I.G.-V., A.F., M.G.N., and J.M. performed research; J.P.S., S.Y.K., M.I.M., A.N., A.F., M.G.N., and J.M. analyzed data; and J.P.S. and J.M. wrote the paper.

The authors declare no competing interest.

This article is a PNAS Direct Submission.



[1]To whom correspondence may be addressed. Email: jmorriso@ucr.edu.

This article contains supporting information online at https://www.pnas.org/lookup/suppl/doi:10.1073/pnas.2300474120/-/DCSupplemental.

Published December 15, 2023.

comprise ~90% of serosal macrophages (18–20). Serosal macrophages have been implicated in organ health. For example, postoperative gastrointestinal dysmotility can be ameliorated in mice by inhibiting peritoneal macrophage functions (21). Furthermore, large peritoneal macrophages enter the liver to promote wound healing in mouse models of sterile liver damage and dextran sulfate sodium (DSS)-induced intestinal colitis (22, 23), while large pericardial macrophages enter the heart to improve immune responses after myocardial infarction (24). However, small serosal macrophages have not been studied in diseases of the visceral organs, and serosal macrophages have never been studied in the context of viral infection.

In this manuscript, we use a systems biology approach as well as traditional "wet lab" techniques to identify a new lung macrophage population that originates in the pleural cavity and promotes recovery from influenza. To achieve this, we combined lung transcriptomic datasets to identify and confirm transcriptomic signatures that distinguish mild and severe influenza outcomes in mice. We then used a tissue deconvolution algorithm known as Digital Cell Quantifier (DCQ) to convert lung transcriptomic data into predictions of immune cell changes that precede different disease outcomes (25). We found that DCQ accurately predicted known cell population dynamics that occurred during influenza infection in vivo and further predicted a lung cell population that transcriptionally resembled small serosal macrophages and whose numbers positively correlated with recovery from influenza.

We used flow cytometry and microscopy to show that fluorescently labeled PMs migrate from the pleural cavity into the lung after infection with a seasonal influenza virus strain, pdmH1N1 A/California/04/2009 (Cal09), after viral clearance has occurred and recovery has been initiated. In line with our DCQ predictions, we found that fewer PM translocated to the lung in mice that were infected with pdmH1N1 A/Netherlands/602/2009 (NL09), which causes more severe disease than Cal09. In addition, PM migration is not mouse strain-specific as both BALB/c and C57BL/6 PMs migrate to the lung in response to IAV infection. We further show that depleting PMs causes increased virus-induced weight loss and a longer recovery time from IAV infection. PM depletion also increases inflammatory cytokine levels in the pleural cavity and lung and increased neutrophil infiltration in the lung after IAV infection.

We show that PMs translocate to the lung during IAV infection and that PMs are important for the resolution of IAV-induced lung disease. We demonstrate the utility of our systems approach for discovering immune cells subsets that correlate with mild and severe disease outcomes. Furthermore, our findings position the pleural cavity as an important contributor to lung homeostasis and the host response to pneumonia.

## Results

**Host Response Differences in Expression of Inflammatory, Metabolic, Cell Cycle, and Tissue Repair Genes Distinguish Influenza Disease Outcomes.** Previously, we identified a gene expression signature in the mouse lung that could distinguish severe and mild influenza (17). We sought to expand our gene expression analysis to a wider range of influenza disease outcomes by including intermediate disease outcomes such as moderate weight loss and severe weight loss with subsequent recovery. Therefore, we integrated transcriptional data from our study (17) with data from an independent study of similar design (26). A description of the two studies and their combined weight loss outcomes are shown (Fig. 1 *A* and *B*). We restricted our analysis to those differentially expressed (DE) genes that had a log fold change of 2 or more with an adjusted *P*-value cut-off of 0.05. When DE genes were clustered based on their biweight midcorrelation (bicor) across samples, six gene expression modules were identified and assigned unique colors (Fig. 1*C*). We then used Ingenuity Pathway Analysis (IPA) to assign functional categories to the genes within each module. The red module was enriched for genes in inflammation-associated pathways such as "Granulocyte adhesion and diapedesis" and "Crosstalk between dendritic cells and natural killer cells". The increased induction of red module transcripts was associated with increased weight loss. The orange module, which had a unique expression pattern, was enriched for genes involved in lipid metabolism ("LXR/RXR activation" and "FXR/RXR activation" pathways) and coagulation. Upregulation of genes in this module on any day post infection in dataset GSE36328 or on day 3 post infection in dataset GSE54048 was associated with survival. Thus, expression patterns of genes within the red and orange modules support our previous observation of perturbations in inflammation, lipid metabolism, and coagulation signaling gene expression (17).

We then characterized the genes in the other four expression modules. The yellow module, which contained genes involved in oxidative stress responses, did not have an obvious pattern that related to weight loss or mortality. The sky-blue module, which contained calcium and actin cytoskeleton signaling genes, also lacked a pattern with regard to weight loss and mortality. Interestingly, upregulation of black module genes on day 3 post infection was associated with infection by H1N1 viruses, but this upregulation was unrelated to weight loss or mortality. The black module contained mitosis and cell cycle control genes. The downregulation of genes in the dark-blue module, which was enriched for tissue repair mechanisms and metabolic response genes, was associated with increased weight loss. We hypothesized that this signature resulted from differential activation or infiltration of immune cells in the lungs of mice that recovered versus those that succumbed to IAV infection.

**Several Immune Cell Types Are Predicted to Correlate with Influenza Disease Severity.** To identify immune cell populations that were potentially associated with the weight loss and mortality outcomes, we employed a tissue deconvolution method known as DCQ. The DCQ algorithm compares the gene expression profiles from 207 different immune cells with whole organ transcriptional data to predict the quantities of immune cells within a complex organ (25). This method utilizes a panel of genes encoding cell surface markers that are commonly used for flow cytometry and whose transcript and protein levels are concordant (25). We took the populations measured by DCQ and used linear regression to identify the cell populations whose numbers were most highly associated with weight loss in infected animals. We identified 26 cell types that were positively or negatively correlated with influenza outcomes (Fig. 2). Loss of stem cell populations as well as lymphoid cells such as immature B and T cells and effector $CD8^+$ T cells was associated with increased weight loss. An increase in monocytes, plasmacytoid dendritic cells (pDCs), and granulocytes was associated with increased weight loss. Though increases in several conventional dendritic cell (cDC) and macrophage populations were associated with increased weight loss and death, the presence of other cDC and macrophage populations was associated with mild disease and recovery. For example, decreases in $CD103^+$ cDCs ($DC.103^+11B^-.LU$) were associated with increased morbidity and mortality. The presence of cells resembling $MHCII^+F4/80^{lo}$ peritoneal macrophages ($MF.II^+480^{lo}.PC$) was associated with mild disease.

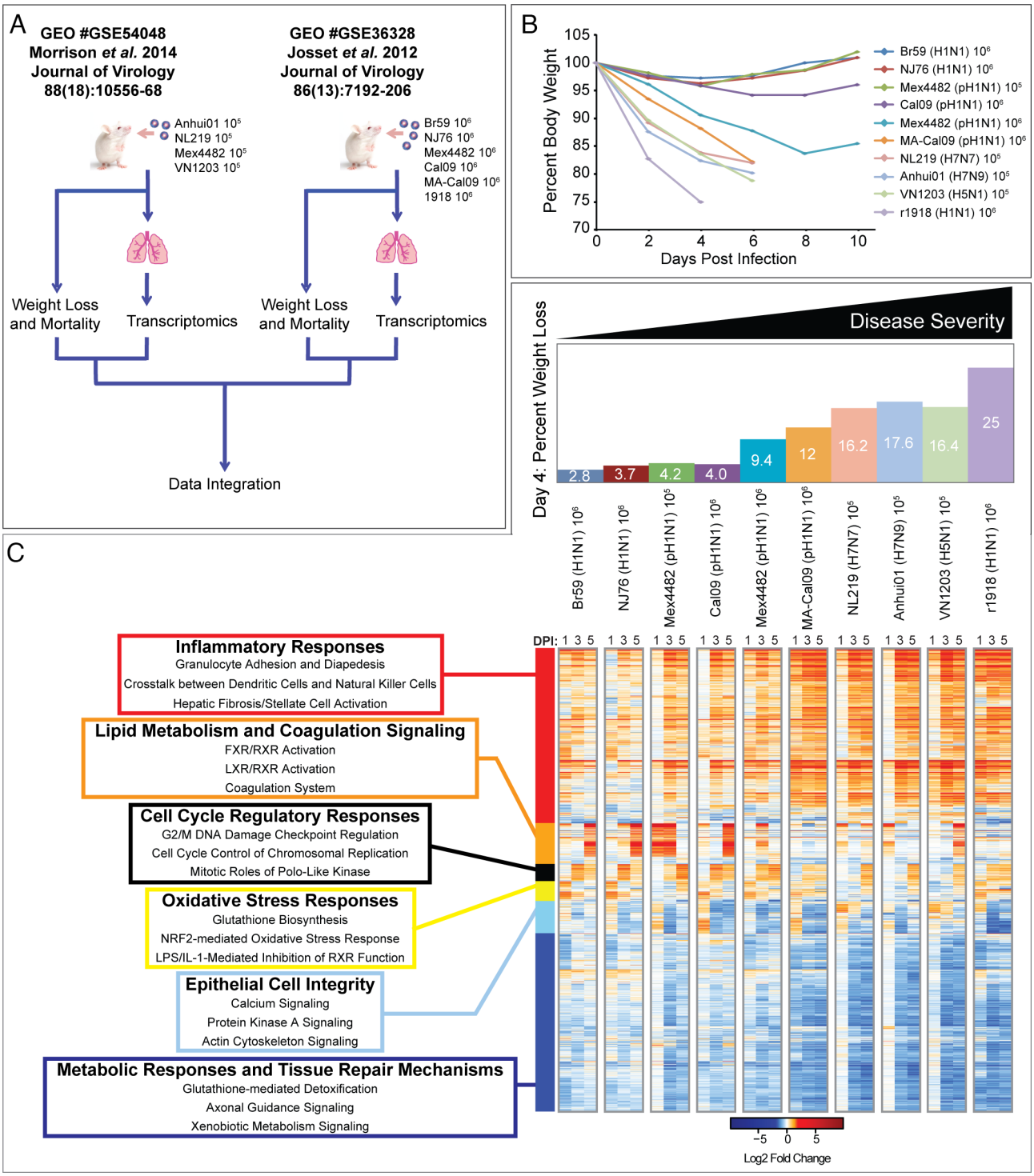


**Fig. 1.** Influenza disease outcomes are distinguished by host response differences in the expression of inflammatory, metabolic, cell cycle, and tissue repair genes. (*A*) Schematic showing the integration of BALB/C mouse data from GSE54048 and GSE36328. Experimental data were combined to produce (*B*) a combined weight loss dataset and a combined transcriptional dataset. (*C*) Hierarchical clustering of differential gene expression in murine lungs infected with influenza virus. Biweight midcorrelation clustering of 6,012 genes that were found to be differentially expressed in any one condition (infection and time). Genes shown in red were up-regulated and genes shown in blue were down-regulated relative to uninfected lungs. Weight loss data shown in (*B*) and (*C*) were obtained from Morrison et al. (17) and Josset et al. (26).

**Immune Cell Predictions Are Conserved across Multiple Transcriptomic Datasets.** To further bolster the tissue deconvolution predictions, we subjected two additional microarray datasets to DCQ. In Shoemaker et al. (GSE63786), C57BL/6 mice were infected with $10^5$ PFU of Cal09 or H5N1 A/Vietnam/1203/2004 (VN1203) IAV and monitored over the course of 7 d (27) (*SI Appendix*, Fig. S1*A*). Lungs from VN1203-infected mice were found to have higher viral loads and more pathology than lungs from Cal09-infected mice (27). In McDermott et al. (GSE33263), C57BL/6 mice were infected with $10^2$, $10^3$, or $10^4$ PFU VN1203 (28) (*SI Appendix*, Fig. S1*B*). Higher inoculation titers led to increased weight loss and mortality (28).

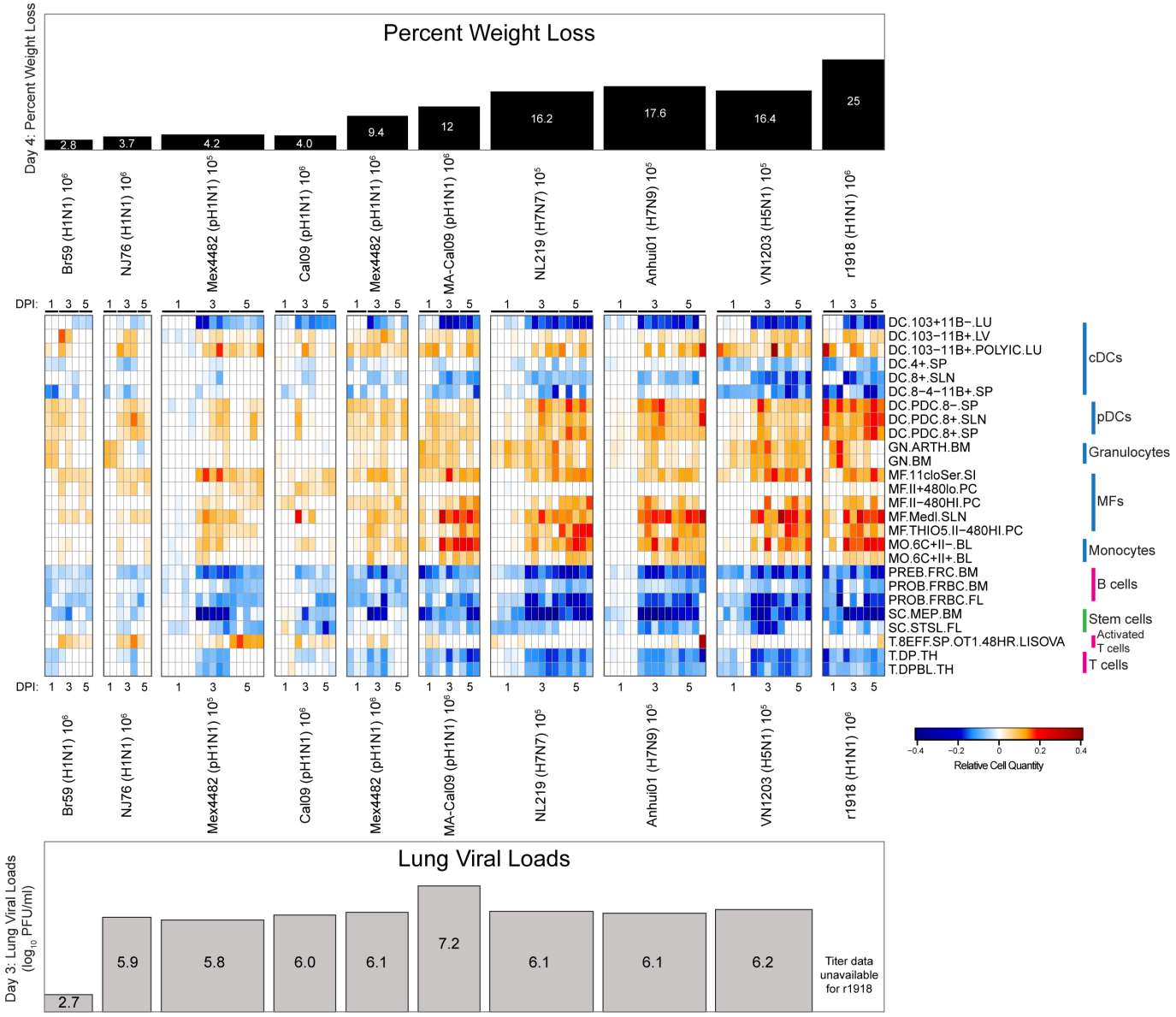


**Fig. 2.** DCQ identified immune cell subsets that predict disease severity or recovery across independent experiments. We surveyed the in vivo dynamics across time and viral strains using the DCQ algorithm. Linear regression models revealed distinct immune cell populations predicted to drive disease morbidity as defined by weight loss following influenza virus infection. The heatmap represents the relative quantity of cell types with significant relationships ($P < 0.05$) between that cell type on at least 1 d to the weights on at least 1 d after filtering for observations where data for at least eight samples were available. Weight loss and viral load data were obtained from Morrison et al. (17) and Josset et al. (26).

When GSE63786 and GSE33263 were run through the DCQ algorithm, we found that the 26 cell types identified from the BALB/c datasets (Fig. 2) largely showed a similar pattern in the C57BL/6 data (*SI Appendix*, Fig. S1 *C* and *D*). As with the BALB/c mice, an increase in monocytes and granulocytes was associated with increased tissue pathology and weight loss in C57BL/6 mice (*SI Appendix*, Fig. S1 *C* and *D*). Loss of stem cell populations, immature B and T cells, and effector $CD8^+$ T cells was also associated with increased weight loss. Again, the presence of cells resembling $MHCII^+F4/80^{lo}$ peritoneal macrophages was associated with mild disease (*SI Appendix*, Fig. S1 *C* and *D*). The only prediction that did not hold across the 4 datasets was that for pDC populations. Higher pDC numbers were associated with severe disease in BALB/c mice (Fig. 2) but were associated with mild disease in C57BL/6 mice (*SI Appendix*, Fig. S1).

**Flow Cytometry Validates DCQ Predictions.** DCQ accurately identified cell population dynamics that have been shown to occur during IAV infection in vivo (Fig. 2 and *SI Appendix*, Fig. S1). For example, $CD103^+CD11b^-$ dendritic cell numbers decrease post infection, modeling what occurs in vivo when they exit the lung and traffic to the draining lymph nodes to present antigen to $CD8^+$ T cells (29, 30).

To further emphasize the value of our approach, we conducted in vivo experiments to confirm some of the predictions. BALB/c mice were infected intranasally with $10^4$ Cal09 virus to induce mild disease or $10^4$ H1N1 A/Puerto Rico/1934 (PR8) virus to induce severe disease. Control mice received PBS intranasally. We isolated, stained, and subjected lung cells to flow cytometry on day 3 post infection. We validated the prediction that more neutrophils and $Ly6C^+$ monocytes were recruited to the lung during

severe disease (*SI Appendix*, Fig. S2) as has been described before (4, 9, 14, 31, 32).

**DCQ Findings Guide the Generation of a Pleural Macrophage-Centered Hypothesis.** Our data thus far supported the idea of a MHCII$^+$F4/80$^{lo}$ macrophage population that originates in a serosal cavity and is present in the lungs of mice that recover from influenza. Since the macrophage populations of the pleural and peritoneal cavities are analogous (18, 20), and the pleural cavity envelopes the lung, we hypothesized that the MHCII$^+$F4/80$^{lo}$ lung macrophages predicted by DCQ originated in the pleural cavity. Though CD11b, CD115, F4/80, and MHCII are sufficient for distinguishing the two pleural macrophage (PM) populations, these markers are insufficient for distinguishing the various macrophage populations in the lung. To circumvent issues with lung macrophage identification, we focused instead on the potential origin of the unique lung population.

**Influenza Virus Infection Promotes the Recruitment of Pleural Macrophages to the Lung.** PMs were labeled in vivo by injecting a red phagocyte-specific dye (PKH26PCL; PKH) into the pleural cavities of mice 1 d prior to infection. When mice were infected intranasally with $10^2$ PFU of Cal09, PKH-labeled cells accumulated in the lung (Fig. 3). Translocated PMs were detected in the lungs on days 6, 9, and 12 post infection, but more accumulation of the PKH$^+$ PMs occurred on 9 and 12 d post infection when compared to the uninfected controls (Fig. 3 *A*–*E*). Flow cytometry gating strategies to distinguish pleural and lung macrophage subpopulations are outlined in *SI Appendix*, Figs. S3 and S4.

PKH$^+$ cells in the lung were mostly CD64$^+$MerTK$^+$SiglecF$^-$CD11b$^+$, which are phenotypically like interstitial macrophages (IMs) (Fig. 3*E*). A smaller pool of PMs were CD64$^+$MerTK$^+$SiglecF$^+$CD11b$^-$, which resemble alveolar macrophages (AMs) (Fig. 3*E*). Heterogeneity amongst IMs has been researched in multiple studies (33–35). One way of distinguishing them is based on their expression of MHCII. We found that the majority of PKH$^+$ lung cells resembled MHCII$^+$ IMs (Fig. 3*E*). Accumulation of this MHCII$^+$CD64$^+$MerTK$^+$SiglecF$^-$CD11b$^+$ population that had originated in the pleural cavity only occurred once animals began to regain weight and after they had cleared virus from their lungs (Fig. 3 *F* and *G*). We also observed an overall increase in the total number of IMs in the lung during IAV infection (Fig. 3 *H*–*J*).

To establish the location of the PKH$^+$ PMs in the lung, frozen lung sections were immunostained and imaged by fluorescence microscopy 9 d post infection (Fig. 4*A*). PKH$^+$ PMs in the lung were detected near the mesothelium (shown by the white dotted line) and within regions of dense DAPI signal (Fig. 4*A*). No PKH$^+$ PMs were detected in the PBS mock-infected control group. To determine whether the migration of PMs occurs through the vasculature, immune cells were isolated from blood on 6, 9, and 12 d post infection. Flow cytometric analysis showed no PKH$^+$ PMs in the blood from either the infected or the control group indicating that the labeled PMs had trafficked through the mesothelium (Fig. 4*B*).

The genetic background of mice can lead to strain-specific differences in PM behavior in steady state and during nematode infection (36). For example, C57BL/6 mice PMs are effective at nematode killing, while BALB/c mice PMs are not (36). Since DCQ predicted a lack of PMs in the lungs of mice infected with pathogenic strains of IAV, we asked whether PM accumulation in the lung would be less efficient during IAV infections that resulted in severe disease. To determine whether IAV-induced PM migration is mouse strain-specific and if it differs based on the virulence of the virus strain used for infection, we injected C57BL/6 J mice intrapleurally with PKH dye, then infected them with 100 PFU of Cal09 or pdmH1N1 A/Netherlands/602/2009 (NL09). We measured PM translocation at 6 DPI because half of the NL09-infected mice reached >25% body weight loss and had to be killed (Fig. 5*A*). PKH$^+$ IMs were detected by flow cytometry in the lungs of both IAV-infected groups at day 6 post infection, but the Cal09-infected mice showed significantly higher accumulation than the PBS control group, while the NL09-infected mice did not (Fig. 5 *B* and *C*). IAV infections led to increased MHCII$^+$ and MHCII$^-$ IM numbers in C57BL/6 J mice (Fig. 5*D*)

Our in vivo labeling of PMs via intrapleural injection of PKH dye is a robust and convenient method for tracking PM movement. PKH dye is widely used in similar experiments and has been shown to efficiently label and distinguish resident cells versus infiltrating cells without affecting the behavior of the labeled cells (23, 37–40). However, there was a possibility that phagocytosis of the PKH dye was inducing PMs to behave aberrantly and translocate to the lung during IAV infection. To exclude this hypothesis, we conducted additional experiments that were not reliant on fluorescently labeling the PMs. Instead, donor cells were pooled from the pleural cavities of C57BL/6 J-*Ptprc*$^{em6Lutzy}$J mice expressing CD45.1$^+$, and PMs were isolated via magnetically activated cell sorting (MACS) using positive selection for CD115$^+$ cells. The donor PMs were then injected into the pleural cavity of recipient C57BL/6 J mice (CD45.2$^+$) 1 d before infection with 100 PFU of Cal09 or mock infected with PBS. Robust accumulation of CD45.1$^+$ PMs was detected in the lungs on day 9 post infection in the Cal09-infected group compared to the mock-infected group (Fig. 5 *E* and *F*). As we had previously seen in the PKH experiments with Balb/C and C57BL/6 J mice, IAV infection led to increases in the MHCII$^+$ and MHCII$^-$ IM populations (Fig. 5*G*).

**Pleural Macrophage Depletion Leads to Increased Weight Loss and Slower Recovery from IAV Infection.** Prior studies have identified roles for serosal cavity macrophages in models of liver, heart, and intestinal injury, showcasing differences in recruitment, wound repair, and weight loss (22–24). A recent study suggested a role for PMs in bacterial clearance in bacterial pneumonia (36). However, no study to date has investigated the role of PMs in viral infection. To test whether PMs affect influenza outcomes, we initially depleted PMs by injecting antibodies against CD115 and compared this to a control IgG-injected group. Mice were injected three times a week for 2 wk then infected with 100 PFU of Cal09. Infected mice receiving anti-CD115 lost more weight compared to the control group, but this difference was not statistically significant (*SI Appendix*, Fig. S5*A*). As this modest effect may have been due to inefficient PM depletion by the CD115 antibody, we compared the level of PM depletion in these animals to what we observed in mice that were intrapleurally injected with clodronate liposomes (CLL) for 24 h (*SI Appendix*, Fig. S5*B*). While anti-CD115 injection depleted just ~50% of PMs, CLL injection depleted ~93% As such, clodronate liposomes (CLL), which deplete macrophages more effectively (*SI Appendix*, Fig. S5*B*), were used to deplete PMs in the rest of this study.

Flow cytometry confirmed that PMs were depleted from 1 d to at least 14 d after intrapleural CLL injection (*SI Appendix*, Fig. S6). Furthermore, intrapleural injection with CLL specifically depleted PMs (*SI Appendix*, Fig. S6). Importantly, macrophage and monocyte populations in the lung-draining lymph nodes (LDLNs) and lungs were unaffected by intrapleural CLL injection (*SI Appendix*, Fig. S6). To test whether PMs affect influenza outcomes, we depleted PMs by injecting CLL into the pleural cavities of mice 1 d prior to infection with Cal09 virus. PM-depleted mice

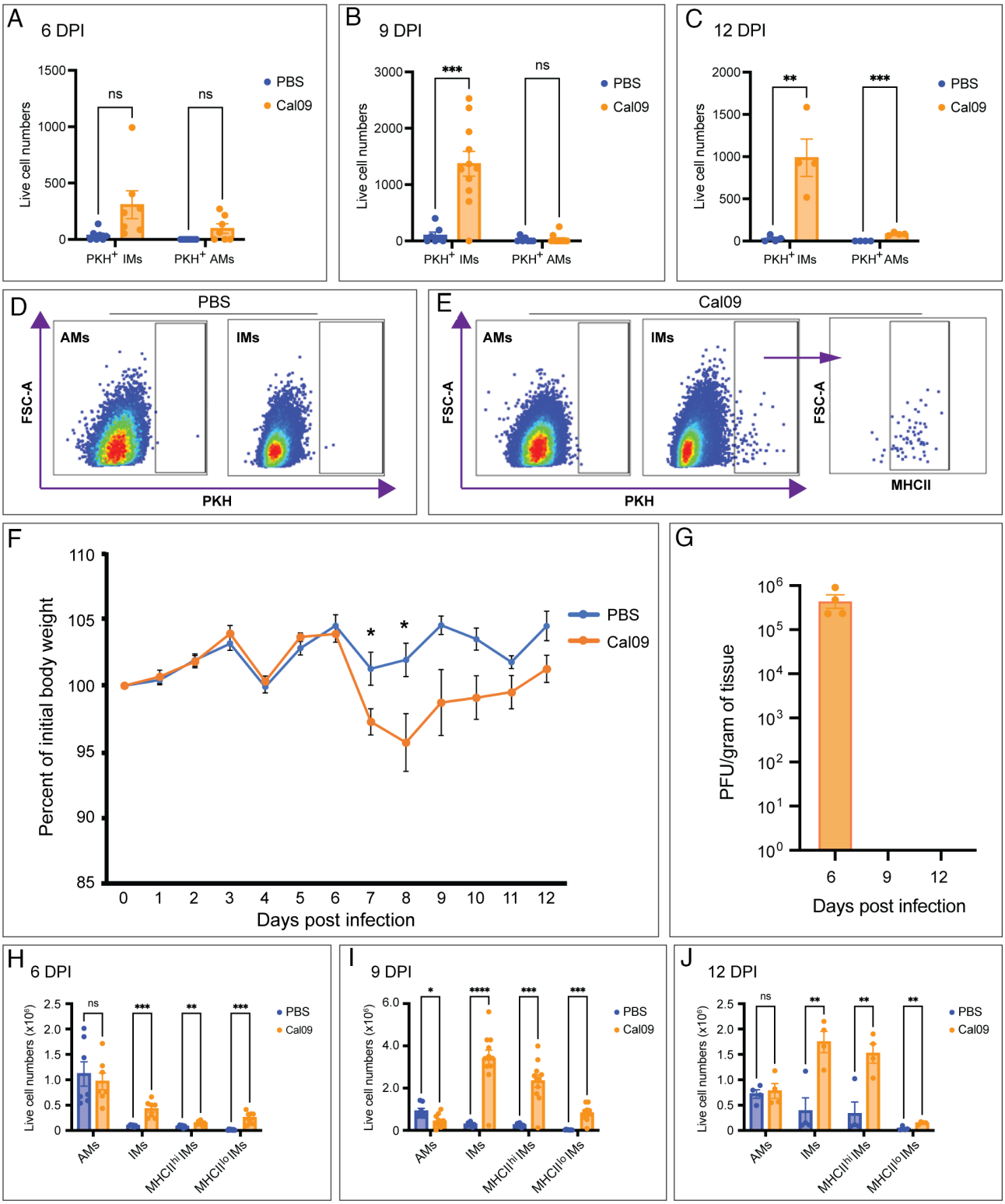


**Fig. 3.** Influenza virus infection promotes the recruitment of pleural macrophages to the lung. BALB/c mice were intrapleurally injected with PKH26PCL (PKH) dye 1 d before they were intranasally infected with $10^2$ PFU Cal09 virus or mock-infected with PBS as a control. (*A–C*) Quantification of live cell numbers of $PKH^+$ AMs and IMs in Cal09- or mock-infected mice. Data are from two independent experiments. (*D*) Representative flow plots of PBS control mice. Data are representative of two independent experiments. (*E*) Representative flow plots of Cal09-infected mice. Data are representative of two independent experiments. (*F*) Weight loss curve of Cal09-infected versus control mice. Data are from two independent experiments. (*G*) Virus titers from lungs of mice in (*F*). (*H–J*) Quantification of live cell numbers of AMs and IMs in Cal09- or mock-infected mice. Data are from two independent experiments. Data shown as mean ± SEM (*$P < 0.05$, **$P < 0.01$, ***$P < 0.001$, Student's *t* test). AM = alveolar macrophage ($MerTK^+CD64^+SiglecF^+CD11b^-$); IM = interstitial macrophage ($MerTK^+CD64^+CD11b^+SiglecF^-$).

lost more weight compared to the PBS liposomes (PBSL)-injected control mice (Fig. 6*A*). However, lung viral loads were unaffected by PM depletion (Fig. 6*B*). Since PM depletion led to more IAV-induced weight loss, and inflammation has been shown to cause appetite suppression, which leads to reduced food intake and causes weight loss (41–43), we asked whether there were increased inflammatory cells and cytokines in the lungs of PM-depleted mice. By measuring the number of $CD45^+$ cells in

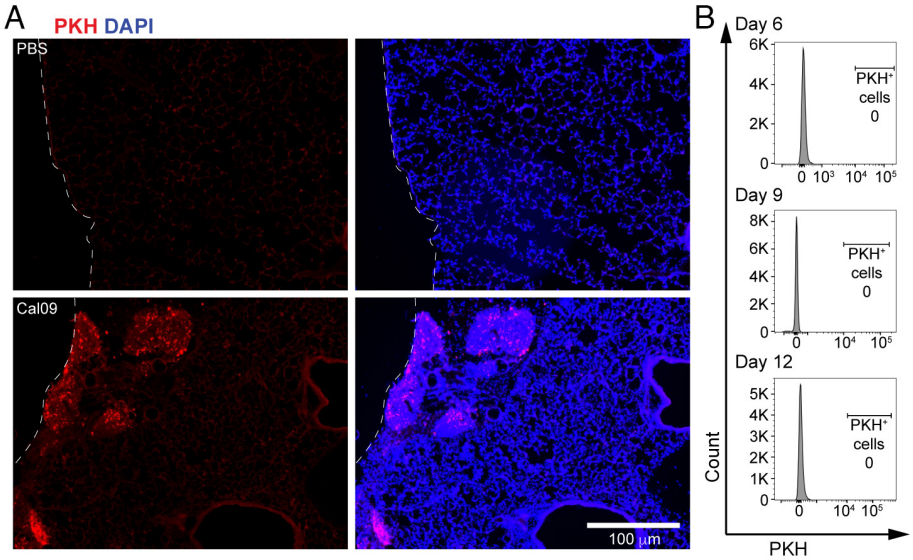


**Fig. 4.** PMs localize near the mesothelium. (*A*) Representative fluorescent images of BALB/c naive and Cal09-infected lungs harvested 9 d post infection. PMs were labeled in vivo with PKH dye (red) and counterstained with DAPI (blue). The mesothelium is outlined by the white dotted line. Data are representative of three independent experiments ($n$ = 8–13 per group). (*B*) Flow cytometry of blood harvested on days 6, 9, and 12 post infection from mice that were intrapleurally injected with PKH26PCL dye then infected with Cal09. Data are representative of two independent experiments.

the lung, we found that the number of total leukocytes in the lungs of PM-deficient and PM-sufficient mice was the same (*SI Appendix*, Fig. S7). However, when we looked at individual leukocyte populations, we found that CLL-treated mice had significantly higher percentages of neutrophils and eosinophils than PBSL-treated mice did on days 3 and 6 post infection (*SI Appendix*, Fig. S7). There were also fewer Ly6C$^{lo}$ monocytes in CLL-treated mice (*SI Appendix*, Fig. S7). However, no significant differences were observed in Ly6C$^{hi}$ monocytes, DCs, and macrophage subsets (*SI Appendix*, Fig. S7). Our flow cytometry gating strategy for distinguishing lung leukocyte populations is outlined in *SI Appendix*, Fig. S8.

PM depletion led to increased lung and pleural cavity inflammation after Cal09 infection as indicated by increased quantities of proinflammatory cytokines: interferon gamma (IFNγ), tumor necrosis factor alpha (TNFα), monocyte chemoattractant protein-1 (MCP-1), interleukin-1 alpha (IL-1α), interleukin-6 (IL-6), and interleukin-1 beta (IL-1β) (Fig. 7*A* and *SI Appendix*, Fig. S9*A*).

Neutrophils were the dominant immune cell population that differentiated PM-sufficient and PM-deficient mice infected with IAV, with neutrophils accumulating to higher levels in the PM-deficient mice (*SI Appendix*, Fig. S7). As such, we asked whether there were any differences in the levels of the neutrophil-associated cytokines, CXCL1, CXCL2, or CCL7, in the lungs and pleural cavity. CXCL1 and CXCL2 have been shown to drive neutrophil recruitment resulting in increased pathogenesis, while CCL7 has been shown to increase monocyte and neutrophil recruitment (44–48). PM depletion did not affect CXCL1, CXCL2, or CCL7 levels in the lungs on days 3, 6, or 9 post infection (Fig. 7*B*). However, CCL7 levels were significantly higher in the pleural fluid of PM-depleted mice on day 9 post infection (*SI Appendix*, Fig. S9*B*). Our data support a model wherein IAV infection of the lung compartment causes cytokine changes in both the lung and pleural cavity. These changes stimulate PMs to move across the mesothelial barrier from the cavity into the lung where they promote recovery from IAV infection by decreasing neutrophil infiltration and inflammation (Fig. 7*C*).

## Discussion

The impact of serosal macrophages on visceral organs has been an understudied area of research. However, a few key studies have described migration of serosal macrophages into visceral organs. These foundational studies focused on sterile injury or inflammation of the liver, heart, and intestine (22–24). Here, we identified a previously unrecognized role for PMs in influenza. We found that IAV infection triggers the recruitment of mature macrophages from the pleural cavity, across the mesothelial layer, and into the lung. PMs are recruited after the clearance of viral infection and when restoration of homeostasis is critical. We observed this by labeling PMs via intrapleural injection of PKH26PCL prior to IAV infection and then measuring their translocation using flow cytometry and immunofluorescence (Figs. 3 and 4). PM translocation was also confirmed with adoptive transfer experiments (Fig. 5). A recent study defined one population of IMs as nerve- and airway-associated macrophages, which express MHCII and proliferate rapidly after IAV infection (49). Our data are supportive of this; we observed a robust increase in the numbers of IMs, most of which are an MHCII$^{hi}$ subpopulation that peaked at 9 d post infection. We show that PMs that translocate to the lung contribute to this MHCII$^{hi}$ IM pool and that this phenomenon is not mouse strain-specific (Figs. 3–5).

Our results differ from those of a recent study that described only surface accumulation of pleural and peritoneal macrophages after organ injury and did not identify a role for serosal macrophages in tissue repair or regeneration (50). This difference may be explained by the timepoints used for observation or by the fact that the researchers only tracked the LPM population. We visualized total PM translocation at late timepoints—during the resolution phase—of a seasonal IAV infection model and showed that PMs affect disease severity. Ablating PMs 1 d prior to infection led to increased weight loss, proinflammatory cytokines, and neutrophil influx in the lungs of IAV-infected mice.

Bénard et al. described increased bacterial burden and mortality upon PM depletion in a mouse model of bacterial pneumonia

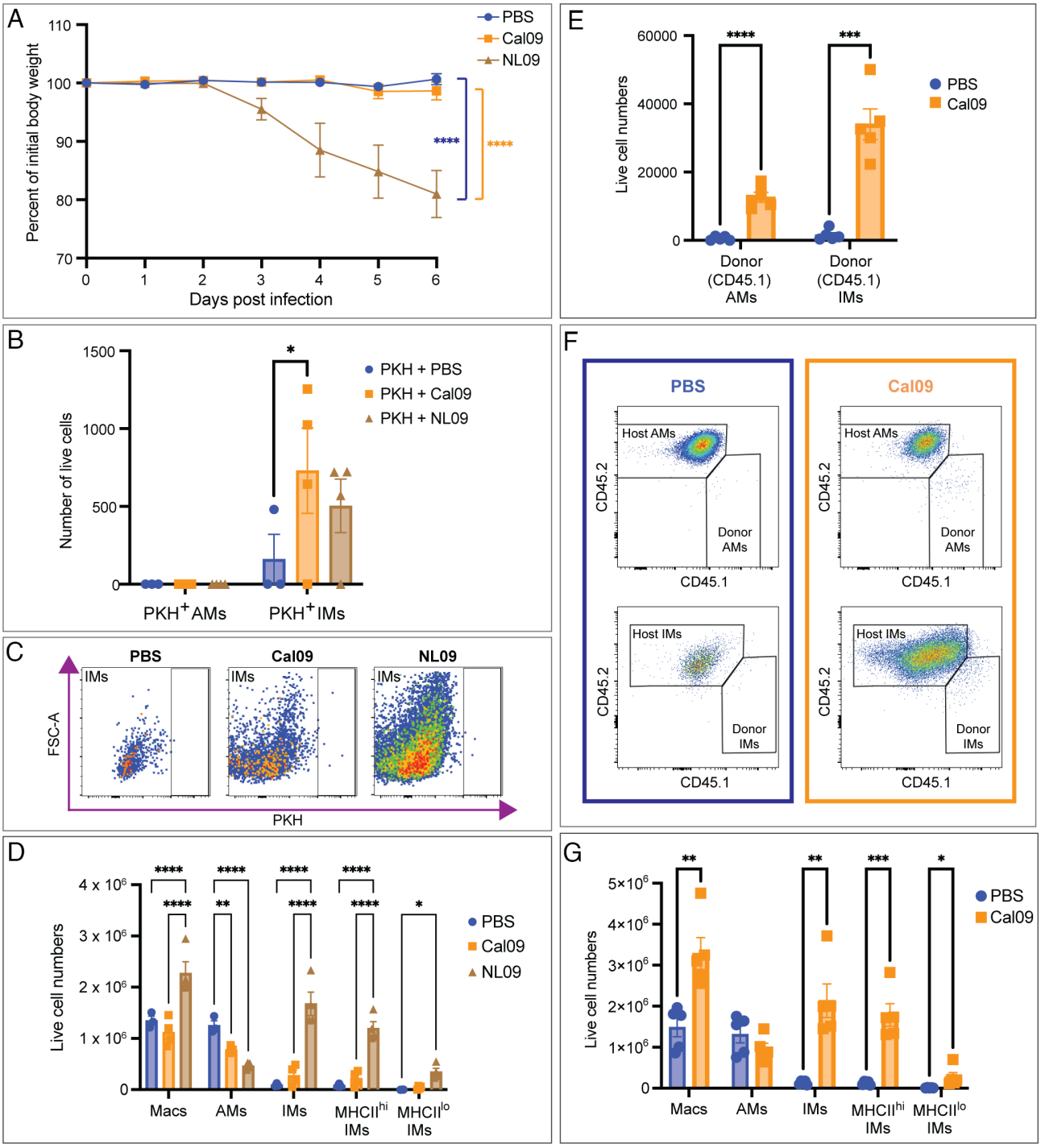


**Fig. 5.** PM migration is not mouse strain specific and PM accumulation occurs predominantly during mild infection. C57BL/6 mice received an intrapleural injection of PKH or PBS 1 d before infection with $10^2$ PFU of Cal09 or NL09 and were sacrificed on day 6 post infection (*A–D*). C57BL/6 received an intrapleural injection of donor CD45.1 (C57BL/6 J- *Ptprc*$^{em6Lutzy}$J) PMs 1 d prior to infection with $10^2$ PFU of Cal09 and were sacrificed on day 9 post infection (*Right*, *E–G*). (*A*) Weight loss was tracked over 6 d post infection ($n$ = 3–4 per group). (*B*) Quantification of live cell numbers of PKH$^+$ AMs and IMs in Cal09-, NL09-, or mock-infected mice. (*C*) Representative flow plots of PBS-, Cal09-, or NL09-infected mice. (*D*) Quantification of live cell numbers of macrophages, AM, and IMs in PBS-, Cal09-, or NL09-infected mice. (*E*) Quantification of live cell numbers of CD45.1$^+$ AMs and IMs. (*F*) Representative flow plots of PBS- or Cal09-infected mice. (*G*) Quantification of live cell numbers of macrophages, AMs, and IMs in PBS-treated or Cal09-infected mice. Data shown as mean ± SEM (*$P$ < 0.05, **$P$ < 0.01, ***$P$ < 0.001, ****$P$ < 0.0001, One-way ANOVA or Student's $t$ test). Mac (MerTK$^+$CD64$^+$) = macrophage; AM = alveolar macrophage (MerTK$^+$CD64$^+$SiglecF$^+$CD11b$^-$); IM = interstitial macrophage (MerTK$^+$CD64$^+$CD11b$^+$SiglecF$^-$).

(51). Unlike in Bénard et al., where bacterial burdens increased upon PM depletion and resulted in increased mortality, we saw increased disease severity without differences in viral titers between PM-depleted and control groups after IAV infection. Additionally, we showed that PMs traffic to the lung after IAV infection, while they did not report PM translocation (51).

An important feature of our study was the use of a systems approach to generate hypotheses. We identified signatures that distinguished mild and severe disease outcomes in mice by combining lung transcriptomic data from two IAV mouse infection studies. We then used tissue deconvolution and linear regression to screen immune populations from the ImmGen database that

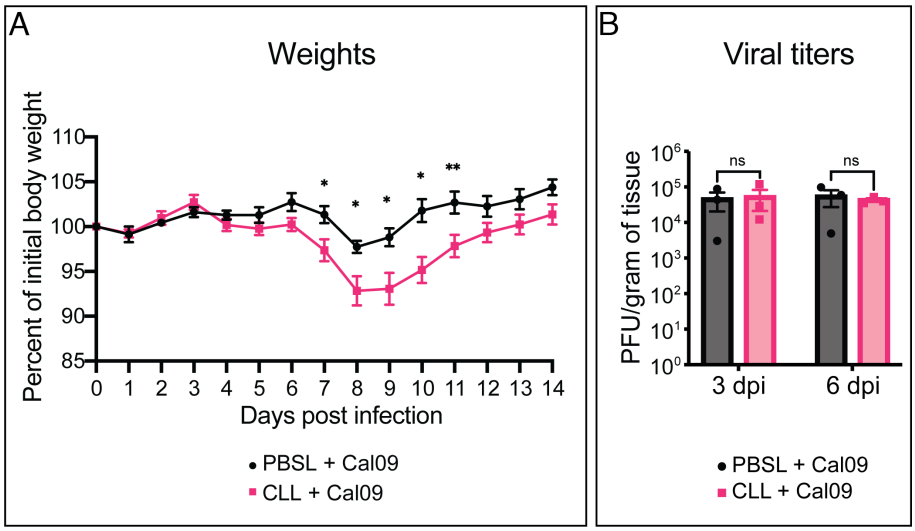


**Fig. 6.** PM depletion increases morbidity in IAV-infected mice. BALB/c mice received an intrapleural injection of CLL or PBSL 1 d before infection with $10^2$ PFU of Cal09; weight loss was tracked and lungs were isolated for viral titers. (*A*) Weight loss was tracked for 14 d after Cal09-infection in both CLL- and PBSL-injected groups. Data are from two independent experiments ($n$ = 10 per group). (*B*) Lung virus titers from CLL- and PBSL-injected mice.

could be driving differences in infection outcomes. Though there is a great deal of heterogeneity amongst lung macrophage populations (19, 20, 33–35, 52), the DCQ algorithm accurately predicted the presence of a population resembling small serosal macrophages that accumulated only in the lungs of animals that survived IAV infection. This prediction was foundational and served as an important tool for identifying a novel immune cell population in our system. Nevertheless, there are limits to tissue deconvolution approaches. Many macrophage populations from different organs share similar phenotypic markers which make it difficult to predict the origin of immune cell populations. In our case, the uniqueness of the small peritoneal macrophage transcriptome in ImmGen was an asset to our predictions and subsequent analyses. As such, characterizing additional immune populations of the serosal cavities and other unique niches will be useful for future predictions.

PMs are important immunomodulators that impact the recovery of IAV-infected mice by decreasing pleural space inflammation and lung neutrophil infiltration (*SI Appendix*, Figs. S7 and S9). Tissue-resident macrophages have been shown to "cloak" proinflammatory debris to contain neutrophil-driven tissue damage and inflammation (53). Furthermore, attenuation of neutrophil influx in IAV infection can improve survival without impacting viral titers (31). Thus, it is feasible that recruited PMs may play a role in masking damage signals to prevent neutrophil infiltration. Pulmonary inflammation can lead to pleural inflammation, which is associated with increased mortality in pneumonia patients and in patients hospitalized with pleural effusion (54, 55). IFNγ levels were higher in both pleural fluid and lungs of IAV-infected, PM-depleted mice (Fig. 7 and *SI Appendix*, Fig. S9). IFNγ deficiency has been shown to decrease susceptibility to lethal infection by increasing activation of group II innate lymphoid cells (ILC2s) (56). We also saw increased MCP-1 in the pleural cavity, and this has been shown to contribute to pleurisy and pleural effusion in carrageenan-induced pleurisy (57).

The pleural cavity may serve as a reservoir for other immune cells that can migrate to the lung. B1a cells, another pleural cavity immune cell population, have important roles in bacterial pneumonia and were shown to migrate to the lung after LPS challenge (58). Furthermore, during IAV infection, pleural cavity B1a cells have important pulmonary responses and are suggested to migrate to infected lungs (59). Whether other pleural cavity cell populations can migrate to the lung has not been determined, but when we looked at other innate immune cell populations, we did not detect $PKH^+$ cells.

The role of the pleural cavity in other viral infections and secondary bacterial infections remains poorly understood. However, meta-analyses of SARS-CoV-2-infected patients showed that pleural effusion was associated with poorer COVID-19 prognoses (60). Similar observations have been seen in patients infected with IAV and/or bacteria (54, 55, 61–63). Additionally, pleural space inflammation can provide protection against bacterial lung infection (51). Following viral infection, patients are left more vulnerable to subsequent pneumonia, but PMs may limit inflammation after infection and decrease susceptibility to pneumonia. There is therefore a need for more research into pleural cavity function in the context of lung infection. Altogether, we show that PMs migrate to the lung during IAV infection and play a role in limiting disease severity by modulating inflammatory responses both in the pleural cavity and in the lung. Selectively targeting PMs could serve as a strategy for treating severe influenza and other lung and pleural diseases. Future studies to understand how PM translocation and plasticity are regulated are warranted.

## Materials and Methods

Please see *SI Appendix, Materials and Methods* for a full description of the methods used.

**Viruses.** pdmH1N1 A/California/04/2009 and H1N1 A/Puerto Rico/8/1934 were gifts from Dr. Adolfo García-Sastre (Icahn School of Medicine at Mount Sinai). pdmH1N1 A/Netherlands/602/2009 virus was a gift from Dr. Rong Hai (University of California, Riverside). Virus stocks were propagated in 8-d-old embryonated eggs (Charles River Laboratories) and titrated by plaque assays on MDCK cells.

The viruses described in Figs. 1 and 2 and *SI Appendix*, Fig. S1 are Br59 = H1N1 (A/Brisbane/59/07); NJ76 = H1N1 A/New Jersey/8/76; Mex4482 = pdmH1N1 (A/Mexico/4482/2009); Cal09 = pdmH1N1 (A/California/04/2009); maCal09 = mouse-adapted pdmH1N1 (A/California/04/2009); NL219 = H7N7 (A/Netherlands/219/2003); Anhui01 = H7N9 (A/Anhui/1/2013); VN1203 = H5N1 (A/Vietnam/1203/2004); 1918 = reconstructed H1N1 (A/South Carolina/1/18).

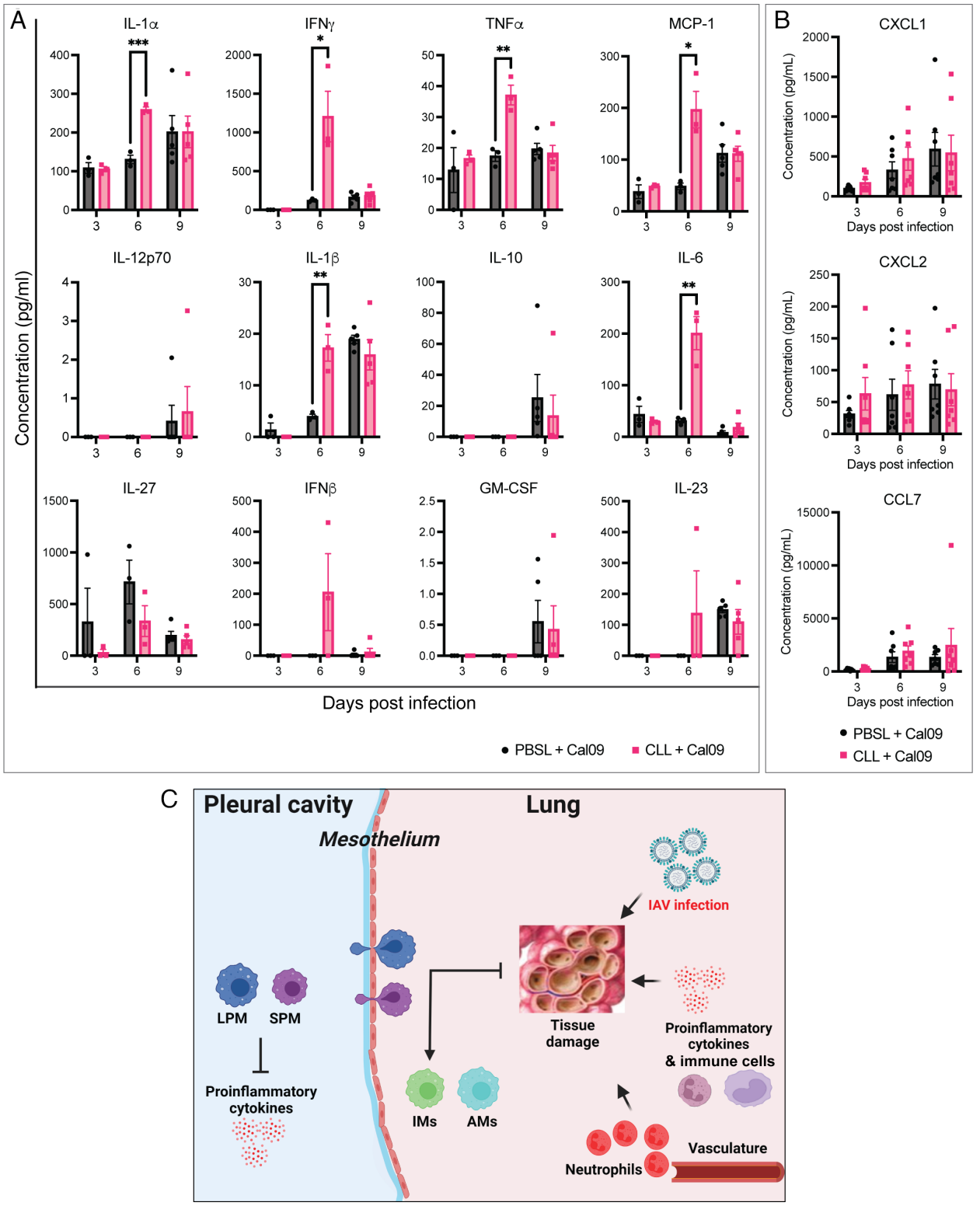


**Fig. 7.** PM depletion leads to increased proinflammatory cytokine levels in the lungs on day 6 post infection. BALB/c mice received an intrapleural injection of CLL or PBSL 1 d before infection with $10^2$ PFU of Cal09 and lungs were isolated on days 3, 6, and 9 post infection. (*A*) Cytokines from lung homogenates. (*B*) Neutrophil-attracting chemokines from lung homogenates. Data are from two independent experiments. (*C*) Proposed model of PM migration to the lung during IAV infection. Data shown as mean ± SEM (*$P$ < 0.05, **$P$ < 0.01, ***$P$ < 0.001, ****$P$ < 0.0001, Student's $t$ test)

**Mouse Experiments.** Female BALB/c, C57BL/6 J, and C57BL/6 J- *Ptprc*$^{em6Lutzy}$J mice, 8 to 12 wk old, were purchased from Jackson Laboratory.

Mice were injected intrapleurally, under isoflurane anesthesia, with 100 μL of 10 μM PKH26PCL (PKH) fluorescent dye (Sigma Aldrich) 1 d before virus infection. In other experiments, mice were injected intrapleurally, under isoflurane anesthesia, with 50 μL of clodronate liposomes or PBS control liposomes (Encapsula Nano Sciences) 1 d before virus infection. Alternatively, mice were injected intrapleurally, under isoflurane anesthesia, with 50 μL of anti-CD115 antibody (BioXcell) or IgG control (BioXcell) three times a week for 2 wk before infection. Mice were challenged intranasally, under isoflurane anesthesia, with 50 μL PBS containing pH1N1 A/California/04/2009, A/Netherlands/602/2009 or H1N1 A/PR/8/1934 viruses, or mock challenged with PBS alone. Lungs were collected and homogenized in 1 mL

PBS and stored at −80 °C until virus titration. Viral titers were measured by plaque assays on MDCK cells.

## Statistics

All results were presented as the mean ± SEM. R and GraphPad Prism 9.4 were used for statistical analyses. The analyses were conducted using Student's $t$ test for comparison between two groups and one-way ANOVA for comparisons between multiple groups ($^{*}P < 0.05$, $^{**}P < 0.01$, $^{***}P < 0.001$, $^{****}P < 0.0001$, and ns for not significant).

## Study Approval

All experiments with mice were performed in accordance with protocols approved by the University of California Riverside Institutional Animal Care and Use Committee.

**Data, Materials, and Software Availability.** All study data are included in the article and/or supporting information. Previously published data were used for this work [GEO datasets GSE54048 (64), GSE36328 (65), GSE63786 (66), and GSE33263 (67)].

**ACKNOWLEDGMENTS.** We thank Maudry Laurent-Rolle, Deborah Spector, Mafalda De Arrabida Farelo, and Xueyan Xu for feedback on this manuscript. We thank Adolfo García-Sastre for providing pdmH1N1 A/California/04/2009 and H1N1 A/Puerto Rico/8/1934 influenza viruses as well as MDCK cells. We thank Rong Hai for providing pdmH1N1 A/Netherlands/603/2009 influenza virus. This research was supported by University of California, Riverside IC funds (to J.M.) and a Regents Faculty Fellowship, University of California (to J.M.).

Author affiliations: [a]Department of Microbiology and Plant Pathology, University of California, Riverside, CA 92521; [b]Division of Biomedical Sciences, School of Medicine, University of California, Riverside, CA 92521; [c]Department of Microbial Infection and Immunity, College of Medicine, The Ohio State University, Columbus, OH 43210; [d]Infectious Diseases Institute, The Ohio State University, Columbus, OH 43210; [e]Department of Microbiology, University of Washington, Seattle, WA 98109; and [f]The Shmunis School of Biomedicine and Cancer Research, George S. Wise Faculty of Life Sciences, Tel Aviv University, Tel Aviv 6997801, Israel

1. T. Horimoto, Y. Kawaoka, Influenza: Lessons from past pandemics, warnings from current incidents. *Nat. Rev. Microbiol.* **3**, 591–600 (2005).
2. P. P. Lamichhane, A. E. Samarasinghe, The role of innate leukocytes during influenza virus infection. *J. Immunol. Res.* **2019**, 8028725 (2019).
3. J. C. Kash *et al.*, Genomic analysis of increased host immune and cell death responses induced by 1918 influenza virus. *Nature* **443**, 578–581 (2006).
4. L. A. Perrone, J. K. Plowden, A. Garcia-Sastre, J. M. Katz, T. M. Tumpey, H5N1 and 1918 pandemic influenza virus infection results in early and excessive infiltration of macrophages and neutrophils in the lungs of mice. *PLoS Pathog.* **4**, e1000115 (2008).
5. K. R. Short, E. J. Kroeze, R. A. Fouchier, T. Kuiken, Pathogenesis of influenza-induced acute respiratory distress syndrome. *Lancet Infect. Dis.* **14**, 57–69 (2014).
6. J. R. Tisoncik *et al.*, Into the eye of the cytokine storm. *Microbiol. Mol. Biol. Rev. (MMBR)* **76**, 16–32 (2012).
7. Writing Committee of the WHO Consultation on Clinical Aspects of Pandemic (H1N1) 2009 Influenza *et al.*, Clinical aspects of pandemic 2009 influenza A (H1N1) virus infection. *N. Engl. J. Med.* **362**, 1708–1719 (2010).
8. S. Herold, C. Becker, K. M. Ridge, G. R. Budinger, Influenza virus-induced lung injury: Pathogenesis and implications for treatment. *Eur. Respir. J.* **45**, 1463–1478 (2015).
9. S. L. Cole *et al.*, M1-like monocytes are a major immunological determinant of severity in previously healthy adults with life-threatening influenza. *JCI Insight* **2**, e91868 (2017).
10. Y. Chi *et al.*, Cytokine and chemokine levels in patients infected with the novel avian influenza A (H7N9) virus in China. *J. Infect. Dis.* **208**, 1962–1967 (2013).
11. M. D. de Jong *et al.*, Fatal outcome of human influenza A (H5N1) is associated with high viral load and hypercytokinemia. *Nat. Med.* **12**, 1203–1207 (2006).
12. Z. Wang *et al.*, Early hypercytokinemia is associated with interferon-induced transmembrane protein-3 dysfunction and predictive of fatal H7N9 infection. *Proc. Natl. Acad. Sci. U.S.A.* **111**, 769–774 (2014).
13. M. Fukushi *et al.*, Serial histopathological examination of the lungs of mice infected with influenza A virus PR8 strain. *PLoS ONE* **6**, e21207 (2011).
14. T. Narasaraju *et al.*, Excessive neutrophils and neutrophil extracellular traps contribute to acute lung injury of influenza pneumonitis. *Am. J. Pathol.* **179**, 199–210 (2011).
15. Z. P. Traylor, F. Aeffner, I. C. Davis, Influenza A H1N1 induces declines in alveolar gas exchange in mice consistent with rapid post-infection progression from acute lung injury to ARDS. *Influenza Other Respir. Viruses* **7**, 472–479 (2013).
16. T. Xu *et al.*, Acute respiratory distress syndrome induced by avian influenza A (H5N1) virus in mice. *Am. J. Respir. Crit. Care Med.* **174**, 1011–1017 (2006).
17. J. Morrison *et al.*, H7N9 and other pathogenic avian influenza viruses elicit a three-pronged transcriptomic signature that is reminiscent of 1918 influenza virus and is associated with lethal outcome in mice. *J. Virol.* **88**, 10556–10568 (2014).
18. C. C. Bain *et al.*, Long-lived self-renewing bone marrow-derived macrophages displace embryo-derived cells to inhabit adult serous cavities. *Nat. Commun.* **7**, ncomms11852 (2016).
19. E. E. Ghosn *et al.*, Two physically, functionally, and developmentally distinct peritoneal macrophage subsets. *Proc. Natl. Acad. Sci. U.S.A.* **107**, 2568–2573 (2010).
20. K. W. Kim *et al.*, MHC II+ resident peritoneal and pleural macrophages rely on IRF4 for development from circulating monocytes. *J. Exp. Med.* **213**, 1951–1959 (2016).
21. T. Maehara *et al.*, Therapeutic action of 5-HT3 receptor antagonists targeting peritoneal macrophages in post-operative ileus. *Br. J. Pharmacol.* **172**, 1136–1147 (2015).
22. M. Honda, M. Kadohisa, D. Yoshii, Y. Komohara, T. Hibi, Directly recruited GATA6+ peritoneal cavity macrophages contribute to the repair of intestinal serosal injury. *Nat. Commun.* **12**, 7294 (2021).
23. J. Wang, P. Kubes, A reservoir of mature cavity macrophages that can rapidly invade visceral organs to affect tissue repair. *Cell* **165**, 668–678 (2016).
24. J. F. Deniset *et al.*, Gata6(+) pericardial cavity macrophages relocate to the injured heart and prevent cardiac fibrosis. *Immunity* **51**, 131–140.e135 (2019).
25. Z. Altboum *et al.*, Digital cell quantification identifies global immune cell dynamics during influenza infection. *Mol. Syst. Biol.* **10**, 720 (2014).
26. L. Josset *et al.*, Implication of inflammatory macrophages, nuclear receptors, and interferon regulatory factors in increased virulence of pandemic 2009 H1N1 influenza A virus after host adaptation. *J. Virol.* **86**, 7192–7206 (2012).
27. J. E. Shoemaker *et al.*, An ultrasensitive mechanism regulates influenza virus-induced inflammation. *PLoS Pathog.* **11**, e1004856 (2015).
28. J. E. McDermott *et al.*, Conserved host response to highly pathogenic avian influenza virus infection in human cell culture, mouse and macaque model systems. *BMC Syst. Biol.* **5**, 190 (2011).
29. A. Ballesteros-Tato, B. Leon, F. E. Lund, T. D. Randall, Temporal changes in dendritic cell subsets, cross-priming and costimulation via CD70 control CD8(+) T cell responses to influenza. *Nat. Immunol.* **11**, 216–224 (2010).
30. J. Helft *et al.*, Cross-presenting CD103+ dendritic cells are protected from influenza virus infection. *J. Clin. Invest.* **122**, 4037–4047 (2012).
31. M. Brandes, F. Klauschen, S. Kuchen, R. N. Germain, A systems analysis identifies a feedforward inflammatory circuit leading to lethal influenza infection. *Cell* **154**, 197–212 (2013).
32. K. L. Lin, Y. Suzuki, H. Nakano, E. Ramsburg, M. D. Gunn, CCR2+ monocyte-derived dendritic cells and exudate macrophages produce influenza-induced pulmonary immune pathology and mortality. *J. Immunol.* **180**, 2562–2572 (2008).
33. S. Chakarov *et al.*, Two distinct interstitial macrophage populations coexist across tissues in specific subtissular niches. *Science* **363**, eaau0964 (2019).
34. S. L. Gibbings *et al.*, Three unique interstitial macrophages in the murine lung at steady state. *Am. J. Respir. Cell Mol. Biol.* **57**, 66–76 (2017).
35. J. Schyns *et al.*, Non-classical tissue monocytes and two functionally distinct populations of interstitial macrophages populate the mouse lung. *Nat. Commun.* **10**, 3964 (2019).
36. C. M. Finlay *et al.*, T helper 2 cells control monocyte to tissue-resident macrophage differentiation during nematode infection of the pleural cavity. *Immunity* **56**, 1064–1081. e1010 (2023).
37. M. Hossain, R. Shim, W. Y. Lee, A. H. Sharpe, P. Kubes, Gata6(+) resident peritoneal macrophages promote the growth of liver metastasis. *Nat. Commun.* **13**, 4406 (2022).
38. P. A. Louwe *et al.*, Recruited macrophages that colonize the post-inflammatory peritoneal niche convert into functionally divergent resident cells. *Nat. Commun.* **12**, 1770 (2021).
39. P. A. Louwe, S. J. Forbes, C. Benezech, C. Pridans, S. J. Jenkins, Cell origin and niche availability dictate the capacity of peritoneal macrophages to colonize the cavity and omentum. *Immunology* **166**, 458–474 (2022).
40. A. S. Neupane *et al.*, Patrolling alveolar macrophages conceal bacteria from the immune system to maintain homeostasis. *Cell* **183**, 110–125.e111 (2020).
41. H. T. Groves, S. L. Higham, M. F. Moffatt, M. J. Cox, J. S. Tregoning, Respiratory viral infection alters the gut microbiota by inducing inappetence. *mBio* **11**, e03236-19 (2020).
42. P. G. Jang *et al.*, NF-kappaB activation in hypothalamic pro-opiomelanocortin neurons is essential in illness- and leptin-induced anorexia. *J. Biol. Chem.* **285**, 9706–9715 (2010).
43. W. Langhans, B. Hrupka, Interleukins and tumor necrosis factor as inhibitors of food intake. *Neuropeptides* **33**, 415–424 (1999).
44. E. E. Hornick *et al.*, Nlrp12 mediates adverse neutrophil recruitment during influenza virus infection. *J. Immunol.* **200**, 1188–1197 (2018).
45. U. Kulkarni *et al.*, Excessive neutrophil levels in the lung underlie the age-associated increase in influenza mortality. *Mucosal Immunol.* **12**, 545–554 (2019).
46. A. Inaba *et al.*, B lymphocyte-derived CCL7 augments neutrophil and monocyte recruitment, exacerbating acute kidney injury. *J. Immunol.* **205**, 1376–1384 (2020).
47. E. S. Choi *et al.*, Enhanced monocyte chemoattractant protein-3/CC chemokine ligand-7 in usual interstitial pneumonia. *Am. J. Respir. Crit. Care Med.* **170**, 508–515 (2004).
48. P. F. Mercer *et al.*, Proteinase-activated receptor-1, CCL2, and CCL7 regulate acute neutrophilic lung inflammation. *Am. J. Respir. Cell Mol. Biol.* **50**, 144–157 (2014).
49. B. B. Ural *et al.*, Identification of a nerve-associated, lung-resident interstitial macrophage subset with distinct localization and immunoregulatory properties. *Sci. Immunol.* **5**, eaax8756 (2020).
50. H. Jin *et al.*, Genetic fate-mapping reveals surface accumulation but not deep organ invasion of pleural and peritoneal cavity macrophages following injury. *Nat. Commun.* **12**, 2863 (2021).
51. A. Benard *et al.*, Pleural resident macrophages and pleural IRA B cells promote efficient immunity against pneumonia by inducing early pleural space inflammation. *Front. Immunol.* **13**, 821480 (2022).
52. S. A. Dick *et al.*, Three tissue resident macrophage subsets coexist across organs with conserved origins and life cycles. *Sci. Immunol.* **7**, eabf7777 (2022).
53. S. Uderhardt, A. J. Martins, J. S. Tsang, T. Lammermann, R. N. Germain, Resident macrophages cloak tissue microlesions to prevent neutrophil-driven inflammatory damage. *Cell* **177**, 541–555.e517 (2019).

54. A. S. Kookoolis, J. T. Puchalski, T. E. Murphy, K. L. Araujo, M. A. Pisani, Mortality of hospitalized patients with pleural effusions. *J. Pulmon. Respir. Med.* **4**, 184 (2014).
55. A. Rosenstengel, Pleural infection–Current diagnosis and management. *J. Thorac. Dis.* **4**, 186–193 (2012).
56. D. Califano *et al.*, IFN-gamma increases susceptibility to influenza A infection through suppression of group II innate lymphoid cells. *Mucosal Immunol.* **11**, 209–219 (2018).
57. S. M. Lansley, H. M. Cheah, Y. C. Lee, Role of MCP-1 in pleural effusion development in a carrageenan-induced murine model of pleurisy. *Respirology* **22**, 758–763 (2017).
58. G. F. Weber *et al.*, Pleural innate response activator B cells protect against pneumonia via a GM-CSF-IgM axis. *J. Exp. Med.* **211**, 1243–1256 (2014).
59. X. Wang *et al.*, IL-17A promotes pulmonary B-1a cell differentiation via induction of Blimp-1 expression during influenza virus infection. *PLoS Pathog.* **12**, e1005367 (2016).
60. S. S. Rathore *et al.*, Prevalence and clinical outcomes of pleural effusion in COVID-19 patients: A systematic review and meta-analysis. *J. Med. Virol.* **94**, 229–239 (2022).
61. N. C. Dean *et al.*, Pleural effusions at first ED encounter predict worse clinical outcomes in patients with pneumonia. *Chest*, 1509–1515 (2016).
62. Y. N. Kim, H. J. Cho, Y. K. Cho, J. S. Ma, Clinical significance of pleural effusion in the new influenza A (H1N1) viral pneumonia in children and adolescent. *Pediatr. Pulmonol.* **47**, 505–509 (2012).
63. P. B. Hasley *et al.*, Do pulmonary radiographic findings at presentation predict mortality in patients with community-acquired pneumonia? *Arch. Intern. Med.* **156**, 2206–2212 (1996).
64. M. Katze *et al.*, Characterizing the transcriptomic response of mice infected with A/Anhui/01/2013 (H7N9), A/Netherlands/219/2003 (H7N7), and A/Vietnam/1203/2004 (H5N1), and a pandemic H1N1 human virus, A/Mexico/4482/2007 (H1N1). GEO. https://www.ncbi.nlm.nih.gov/geo/query/acc.cgi?acc=GSE54048. Accessed 13 January 2014.
65. L. Josset *et al.*, IM002, IM009 - Implication of inflammatory macrophages, nuclear receptors and interferon regulatory factors in increased virulence of pandemic 2009 H1N1 influenza A virus after host adaptation. GEO. https://www.ncbi.nlm.nih.gov/geo/query/acc.cgi?acc=GSE36328. Accessed 7 March 2012.
66. J. E. Shoemaker *et al.*, An ultrasensitive mechanism regulates influenza virus-induced inflammation. GEO. https://www.ncbi.nlm.nih.gov/geo/query/acc.cgi?acc=GSE63786. Accessed 2 December 2014.
67. C. Li *et al.*, IM001: Influenza A/VN/1203/04 infection of C57Bl/6 mouse model - Data from 3 viral doses at 1, 2, 4 and 7 days post infection. GEO. https://www.ncbi.nlm.nih.gov/geo/query/acc.cgi?acc=GSE33263. Accessed 26 October 2011.